ISSN: 2710-0588

Low-Carbon Economic Dispatch of Power Grid with Electric Vehicles Considering Wind Power Accommodation

Liangliang Sun[1,*], Xingguo Tan[1], Chaomeng Li[1]

[1]School of Electrical Engineering and Automation, Henan Polytechnic University, Jiaozuo Henan 454000, China

[*] Corresponding Author: sll15236861762@163.com

Abstract

To mitigate the impact of uncoordinated charging of electric vehicle (EV) clusters on grid load and improve wind power accommodation, this paper proposes an ordered charging scheduling strategy for EVs considering wind power consumption. First, a charging load model for EVs is established, and the impact of uncoordinated charging of EV clusters of different scales on grid load is analyzed. Second, an ordered charging control model for EV clusters is developed, and a time-of-use (TOU) electricity price strategy based on grid-connected wind power output is proposed to effectively regulate the charging load of EVs and battery charging and swapping stations (BCSS), thereby enhancing wind power accommodation. Finally, considering carbon trading and wind curtailment penalty costs, a low-carbon economic dispatch model for the power grid is established, aiming to minimize both the load peak-valley difference and the comprehensive operating cost. The NSGA-II algorithm is employed to solve the model. Simulation results demonstrate that the proposed strategy can increase wind power accommodation while achieving low-carbon and economic operation of the grid.

Keywords

Wind power accommodation, electric vehicle, charging/swapping station, NSGA-II.

1. Introduction

With the rapid proliferation of electric vehicles (EVs), investigating how to achieve a positive interaction between EVs and renewable energy generation to promote energy conservation and emission reduction has become a key initiative for realizing the "dual carbon" goals [1-2]. EV power batteries, predominantly lithium-based, serve as controllable distributed energy storage devices that can be used to absorb renewable energy generation [3-4]. However, the charging of EVs in the power grid represents random and uncertain load. The increasing number of EVs inevitably poses significant challenges to the stable and secure operation of the grid [6-8].

Ref. [9] addresses the uncertainty of EV charging load by integrating electricity price information with traffic conditions and charging station queue status. Through a vehicle-to-grid (V2G) platform, optimal charging schemes are pushed to users, effectively dispersing the temporal distribution of charging load and reducing congestion probability during peak charging periods. Ref. [10] proposes a hierarchical and zonal coordinated charging/discharging control architecture for EVs. This strategy aggregates and pre-schedules charging load at the regional level, performs rolling corrections based on real-time operating status, and enables active response of EV clusters to peak-shaving demands of distribution networks. Ref. [11] constructs a prospect-theory-based response model of EV users to TOU electricity prices. By analyzing the transition probabilities of users' charging periods under different price differentials, the study quantifies the nonlinear relationship between price incentives and

ISSN: 2710-0588

actual user behavior. Ref. [12] focuses on wind power accommodation and proposes a dynamic TOU electricity price optimization method linked to wind power forecast. By dynamically dividing peak, flat, and valley periods and adjusting price differentials, simulation results show that this method can increase wind power accommodation by approximately 15% compared to conventional TOU tariffs, while also demonstrating its effectiveness in peak shaving and valley filling.

However, most existing studies fail to consider the close coupling between renewable energy output and EV charging from a low-carbon perspective. Therefore, based on analyzing the impact of uncoordinated charging of EV clusters of different scales on grid load, this paper establishes an ordered charging control model for EV clusters, formulates a TOU electricity price strategy based on the magnitude of grid-connected wind power, and effectively regulates the charging load of EVs and BCSS. To reduce carbon emissions from thermal power units in the grid, carbon trading and wind curtailment penalty costs are introduced, and a low-carbon economic dispatch model aiming to minimize both the load peak-valley difference and the comprehensive operating cost is developed. The NSGA-II algorithm is used to solve the model. Simulation results show that the proposed strategy can increase wind power accommodation and achieve low-carbon economic operation of the grid.

2. Modeling

2.1. EV Charging Load Model

Many factors influence EV charging load, which for simplicity can be categorized into three types: charging method, battery characteristics, and user behavior [13-15]. This paper adopts AC slow charging for EVs, and the charging process is simplified and approximated as constant-power charging [16].

The state of charge (SOC) of an EV battery during charging is expressed as:

$$SOC_{\mathrm{EV}}(t) = SOC_{\mathrm{EV}}(t-1) + \frac{1}{E_{\mathrm{EV,rat}}}\int_{t-1}^{t} P_{\mathrm{EV}}^{\mathrm{cha}}(t)\eta_{\mathrm{EV}}^{\mathrm{cha}}dt \tag{1}$$

where $SOC_{\mathrm{EV}}(t)$ is the SOC of the EV battery at time t, $E_{\mathrm{EV,rat}}$ is the rated capacity of the battery, $P_{\mathrm{EV}}^{\mathrm{cha}}(t)$ is the charging power of the EV battery, $\eta_{\mathrm{EV}}^{\mathrm{cha}}$ is the charging efficiency of the EV battery.

Ref. [17] statistically analyzes a large number of EV user behaviors, indicating that the main factors influencing charging demand are daily driving distance, charging start time, and charging end time. Fitting based on statistical results yields: the daily driving distance approximately follows a lognormal distribution, while charging start time and charging end time approximately follow normal distributions.

$$f(t_{\mathrm{in}}) = \begin{cases} \dfrac{1}{\sigma_b\sqrt{2\pi}}\exp[-\dfrac{(t_{\mathrm{in}}+24-\mu_b)^2}{2\sigma_b^2}], 1 < t_{\mathrm{in}} \le \mu_b - 12 \\ \dfrac{1}{\sigma_b\sqrt{2\pi}}\exp[-\dfrac{(t_{\mathrm{in}}-\mu_b)^2}{2\sigma_b^2}], \mu_b - 12 < t_{\mathrm{in}} \le 24 \end{cases} \tag{2}$$

$$f(s) = \frac{1}{s\sigma_s\sqrt{2\pi}}\exp[-\frac{(\ln s-\mu_s)^2}{2\sigma_s^2}] \tag{3}$$

ISSN: 2710-0588

$$f(t_{out})=\begin{cases}\frac{1}{\sigma_a\sqrt{2\pi}}\exp[-\frac{(t_{out}-\mu_a)^2}{2\sigma_a^2}], 1<t_{out}\le\mu_a+12\\ \frac{1}{\sigma_a\sqrt{2\pi}}\exp[-\frac{(t_{out}-\mu_a-24)^2}{2\sigma_a^2}], \mu_a+12<t_{out}\le\mu_a+24\end{cases} \tag{4}$$

where t_{in} is the charging start time, expected value μ_b= 17.6, standard deviation σ_b= 3.2. s is the daily driving distance, expected value μ_s= 32, standard deviation σ_s= 0.88. t_{out} is the charging end time, expected value μ_a= 7.58, standard deviation σ_a= 3.87.

From the above analysis, the SOC of an EV when it ends its trip and connects to the grid to start charging can be expressed as:

$$SOC_{EV}(t_{in})=SOC_{EV}(t_{out})-\frac{s\bullet\gamma}{E_{EV,rat}} \tag{5}$$

where $SOC_{EV}(t_{in})$ denotes the SOC of the EV battery at the start of charging; $SOC_{EV}(t_{out})$ denotes the SOC at the end of charging; γ denotes the electricity consumption per kilometer.

Assuming that the replacement batteries provided by the BCSS have parameters consistent with EV batteries, combining Eq. (1)–(5), the charging duration of EVs and the equivalent total uncoordinated charging load of EVs and BCSS can be derived as:

$$\begin{cases}T^{cha}(t)=\frac{s\bullet\gamma}{P_{EVx}^{cha}(t)\bullet\eta_{EV}^{cha}}\\ SOC_{x,des}\le SOC_{x,end}\le SOC_{x,max}\\ P_{BCSS}(t)=\sum_{x=1}^{X}P_{EVx}^{cha}(t)+\sum_{y=1}^{Y}P_{CSy}(t)\end{cases} \tag{6}$$

where $T^{cha}(t)$ is the charging duration of the EV battery, $SOC_{x,end}$ is the SOC of after charging. To meet user demand, it must reach the desired $SOC_{x,des}$ and not exceed the maximum $SOC_{x,max}$, $P_{BCSS}(t)$ is the total load of EVs and BCSS, $P_{CSy}(t)$ is the charging power of replacement battery y providing battery swapping service [18].

2.2. Ordered Charging Control Model for EVs

Since EV power batteries are expensive, to avoid additional battery life loss caused by discharging during dispatch – which would discourage user participation – this paper only considers ordered charging control. The energy variation of an EV with and without participation in ordered charging scheduling is shown in Fig. 1.

As shown in Fig. 1, when the user does not participate in scheduling, the energy variation can be represented by the broken line *a-b-c*. The slope of line *a-b* is the rated charging power, and line *b-c* is horizontal, indicating no charging action, i.e., charging reaches the desired or full state. It can be seen that without scheduling, the EV charges at the rated power from the time it connects to the grid after the trip t_{in} until it disconnects at t_{out}. During the period from the time it reaches the desired/full state t_{sp} to departure time t_{out}, the EV is not effectively utilized. When the user participates in scheduling, the broken line *a-b-c* represents the upper bound of the cumulative charging energy under scheduling; the broken line *a-d-c* represents the lower bound. The horizontal line *a-d* indicates delayed charging (no action), and line *d-c* has slope equal to the rated charging power, meaning that after connection, charging is delayed until it starts at the rated power to reach the desired/full state $E_{EV,end}$ by departure. The region *a-b-c-d*

ISSN: 2710-0588

is the charging scheduling boundary of the EV. Any broken line within this region (horizontal or rising) represents a feasible ordered charging schedule, such as the line *a-e-f-g-c*.

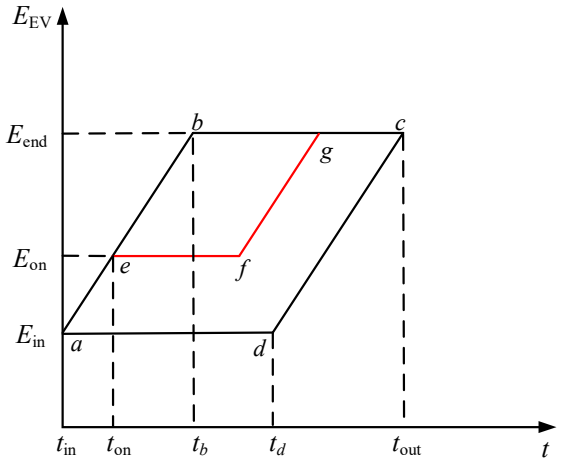

Figure 1. Energy changes when EVs are charged

From the above analysis, the charging scheduling constraints and the cumulative energy boundary for the x-th EV participating in scheduling are:

$$\begin{cases} 0 \le P_{\mathrm{EV}x,t}^{\mathrm{cha}} \le P_{\mathrm{EV}}^{\mathrm{cha,max}} \\ E_{\mathrm{EV}x,\mathrm{in}} \le E_{\mathrm{EV}x,t} = E_{\mathrm{EV}x,t-1} + \eta_{\mathrm{EV}}^{\mathrm{cha}} P_{\mathrm{EV}x,t}^{\mathrm{cha}} \Delta t \le E_{\mathrm{EV}x,\mathrm{end}} \end{cases} \tag{7}$$

$$E_{\mathrm{EV}x,t}^{\mathrm{ch,max}} = \begin{cases} (t - t_{x,\mathrm{in}}) \eta_{\mathrm{EV}}^{\mathrm{cha}} P_{\mathrm{EV}x}^{\mathrm{cha,max}} \Delta t, t_{x,\mathrm{in}} \leqslant t < t_{x,b} \\ E_{\mathrm{EV}x,\mathrm{out}} - E_{\mathrm{EV}x,\mathrm{in}}, t_{x,b} \leqslant t \leqslant t_{x,c} \end{cases} \tag{8}$$

where $P_{\mathrm{EV}}^{\mathrm{cha,max}}$ is the rated charging power of the EV; $E_{\mathrm{EV}x,t}^{\mathrm{ch,max}}$ is the maximum cumulative chargeable energy of *x*.

The scheduling time parameters are respectively:

$$\begin{cases} t_{x,b} = t_{x,\mathrm{in}} + \dfrac{E_{\mathrm{EV}x,\mathrm{out}} - E_{\mathrm{EV}x,\mathrm{in}}}{\eta_{\mathrm{EV}}^{\mathrm{cha}} P_{\mathrm{EV}x}^{\mathrm{cha,max}}} \\ t_{x,d} = t_{x,\mathrm{out}} - \dfrac{E_{\mathrm{EV}x,\mathrm{out}} - E_{\mathrm{EV}x,\mathrm{in}}}{\eta_{\mathrm{EV}}^{\mathrm{cha}} P_{\mathrm{EV}}^{\mathrm{cha,max}}} \end{cases} \tag{9}$$

where $t_{x,\mathrm{in}}$, $t_{x,\mathrm{out}}$, $E_{\mathrm{EV}x,\mathrm{in}}$, $E_{\mathrm{EV}x,\mathrm{out}}$ can be derived from EV user characteristics and Monte Carlo simulation[19].

In summary, the set of dispatchable domain parameters for the *x*-th EV is:

$$W_{\mathrm{EV}x} = \left\{ P_{\mathrm{EV}x,t}^{\mathrm{cha}}, E_{\mathrm{EV}x,t}^{\mathrm{cha,max}} \middle| \forall t \in T_{\mathrm{EV}x} \right\} \tag{10}$$

where $T_{\mathrm{EV}x}$ is the set of scheduling time parameters for the *x*-th EV.

Using Minkowski addition to aggregate the individual dispatchable domains of EVs[20], the dispatchable domain parameters of the EV cluster are obtained as:

ISSN: 2710-0588

$$\begin{cases} P_{\mathrm{EV},t}^{\mathrm{cha,max}} = \sum_{x} Z_{x,t} P_{\mathrm{EV}x}^{\mathrm{cha,max}} \\ E_{\mathrm{EV},t}^{\mathrm{cha,max}} = \sum_{x} E_{\mathrm{EV}x}^{\mathrm{cha,max}} \end{cases} \tag{11}$$

$$W_{\mathrm{EV}} = \left\{ P_{\mathrm{EV},t}^{\mathrm{ch,max}}, E_{\mathrm{EV},t}^{\mathrm{ch,max}} \middle| \forall t \in T_{\mathrm{EV}} \right\} \tag{12}$$

where $Z_{x,t}$ is the state of the x-th EV in period t, a 0-1 variable. Z= 1 indicates the EV can be scheduled, Z= 0 indicates not schedulable.

3. Dynamic TOU Electricity Pricing Strategy

The TOU electricity pricing mechanism, leveraging cost differences, is well-suited for regulating ordered charging of EV clusters. To strengthen the coupling between EVs and wind power, particularly to enhance wind power accommodation, this paper proposes a dynamic TOU electricity pricing strategy that considers wind power consumption.

The dynamic TOU electricity price based on wind power accommodation can be expressed as:

$$P_{\mathrm{wind,av}} = \frac{1}{T} \sum_{t=1}^{T} P_{\mathrm{wind,pre}}(t) \tag{13}$$

$$C_{\mathrm{EV}}(t) = \begin{cases} (1+0.6)c_0, P_{\mathrm{wind}}(t) < (1-0.25) P_{\mathrm{wind,av}} \\ c_0, (1-0.25) P_{\mathrm{wind,av}} \le P_{\mathrm{wind}}(t) \le (1+0.25) P_{\mathrm{wind,av}} \\ (1-0.6)c_0, (1+0.25) P_{\mathrm{wind,av}} < P_{\mathrm{wind}}(t) \end{cases} \tag{14}$$

where $P_{\mathrm{wind,pre}}$ is the forecasted grid-connected wind power output, $P_{\mathrm{wind,av}}$ is the average wind power output, c_0 is the base electricity price of the grid, $C_{\mathrm{EV}}(t)$ is the EV charging electricity price in period t.

It should be noted that both high and low electricity prices are floated based on the base electricity price [21], with the floating amplitude not exceeding 60% of the base price.

4. Grid Load Evaluation Indicators

This paper mainly introduces the following grid load evaluation indicators to analyze the impact of EV cluster charging load.

(1) Peak and valley values

During power system operation, the maximum load value occurring in a certain period is called the load peak; the minimum load value is called the load valley.

(2) Peak-valley difference rate

The peak-valley difference rate φ reflects the load fluctuation level of the grid and is calculated as:

$$\varphi = \frac{P_{\mathrm{peak}} - P_{\mathrm{vall}}}{P_{\mathrm{peak}}} \times 100\% \tag{15}$$

where P_{peak} and P_{vall} are the load peak and valley values.

(3) Load variance

ISSN: 2710-0588

Load variance σ^2 is an important indicator for evaluating grid stability and load fluctuation, calculated as:

$$\begin{aligned}\sigma^2 &= \int_0^T \left[P_{\text{load}}(t) - \frac{1}{T}\int_0^T P_{\text{load}}(t)dt \right] dt \\ &= \int_0^T \left[P_{\text{load}}(t) - P_{\text{av}} \right]^2 dt\end{aligned} \tag{16}$$

where $P_{\text{load}}(t)$ is the total grid load at time t, P_{av} is the average load over the time period T.

5. Low-Carbon Economic Dispatch Model

The low-carbon economic dispatch model aims to minimize both the load peak-valley difference and the comprehensive operating cost. Carbon trading costs and wind curtailment penalty costs are introduced, and constraints of each generating unit are comprehensively considered. Through orderly regulation of the charging load of EV clusters and BCSS as well as the output of thermal power units, low-carbon economic operation of the grid is achieved.

5.1. Objective Functions

To reduce system complexity, thermal power units only account for generation costs (including operation and maintenance costs) and carbon trading costs. Additionally, thermal power units are required to provide a certain capacity of spinning reserve [22] to cope with wind power and load fluctuations. Wind power only accounts for operation and maintenance costs and wind curtailment penalty costs. The BCSS only accounts for the depreciation cost of replacement batteries. It should be noted that actual grid operation also needs to consider factors such as market fuel price fluctuations, grid losses, and other investment costs [23-25].

Objective function 1: Minimize grid load peak-valley difference

$$F_1 = \min[P_{\text{peak}}(t) - P_{\text{vall}}(t)] \tag{17}$$

Objective function 2: Minimize comprehensive operating cost

$$F_2 = \min(C_{\text{wind}} + C_{\text{th}} + C_{\text{BCSS}} + C_{\text{tran}} + C_{\text{r}}) \tag{18}$$

where C_{wind} is the operation and maintenance cost of wind turbines, C_{th} is the generation cost of thermal power units, C_{BCSS} is the operation and maintenance cost of the BCSS, C_{tran} is the carbon trading cost, C_{r} is the spinning reserve cost.

The calculation of C_{wind} is:

$$C_{\text{wind}} = \sum_{t=1}^{T} k_1 P_{\text{wind}}(t) + \sum_{t=1}^{T} k_2 [P_{\text{wind,pre}}(t) - P_{\text{wind}}(t)] \tag{19}$$

where k_1 is the unit operation and maintenance cost coefficient for wind power, k_2 is the unit wind curtailment penalty cost coefficient.

The calculation of C_{th} is:

$$C_{\text{th}} = \sum_{t=1}^{T}\sum_{m=1}^{M} [a_m P_{\text{th},m}^2(t) + b_m P_{\text{th},m}(t) + c_m] \tag{20}$$

ISSN: 2710-0588

where a_m, b_m, c_m are the cost coefficients of thermal unit m.
The calculation of C_{BCSS} is:

$$C_{\mathrm{BCSS}} = k_{\mathrm{bat}} \sum_{y}^{Y} P_{\mathrm{CSy}}(t) \tag{21}$$

where k_{bat} is the depreciation cost coefficient of replacement batteries in the station.
The calculation of C_{tran} is:

$$\begin{cases} Q_{\mathrm{th,q}} = \sum_{t=1}^{T} \sum_{m=1}^{M} \varepsilon_{m,\mathrm{q}} P_{\mathrm{th},m}(t) \\ Q_{\mathrm{th}} = \sum_{t=1}^{T} \sum_{m=1}^{M} \varepsilon_{m} P_{\mathrm{th},m}(t) \\ C_{\mathrm{tran}} = \psi (Q_{\mathrm{th}} - Q_{\mathrm{th,q}}) \end{cases} \tag{22}$$

where $Q_{\mathrm{th,q}}$ is the carbon emission quota of thermal power units, $\mathrm{Q_{th}}$ is the actual carbon emission of thermal power units, M is the number of thermal power units, $P_{\mathrm{th},m}(t)$ is the actual power of thermal unit m in period t, $\varepsilon_{m,\mathrm{q}}$ is the quota coefficient of thermal unit m, ε_m is the actual emission coefficient of thermal unit m, ψ is the unit carbon emission trading price.
The calculation of C_{r} is:

$$C_{\mathrm{r}}(t) = \sum_{m=1}^{M} [P_{\mathrm{th},m,\mathrm{up}}(t) + P_{\mathrm{th},m,\mathrm{dn}}(t)] c_{\mathrm{r}} \tag{23}$$

where c_{r} is the cost coefficient of spinning reserve capacity, $P_{\mathrm{th},m,\mathrm{up}}(t)$ and $P_{\mathrm{th},m,\mathrm{dn}}(t)$ are the upward and downward spinning reserve capacities provided by thermal unit m.

5.2. Constraints

In addition to the ordered charging scheduling constraints for EV clusters, other constraints in the system are:
(1) Power balance constraint

$$P_{\mathrm{wind}}(t) + P_{\mathrm{th}}(t) = P_{\mathrm{base}}(t) + P_{\mathrm{BCSS}}(t) \tag{24}$$

where $P_{\mathrm{base}}(t)$ is the grid base load, $P_{\mathrm{th}}(t)$ is the actual output of thermal power units.
(2) Generating unit power constraints

$$\begin{cases} P_{\mathrm{wind}}^{\max}(t) = P_{\mathrm{grid}}(t) + P_{\mathrm{wind,q}}(t) \\ 0 \le P_{\mathrm{grid}}(t) \le P_{\mathrm{wind}}^{\max}(t) \end{cases} \tag{25}$$

where $P_{\mathrm{wind}}^{\max}(t)$ denotes the maximum output power of the wind farm, $P_{\mathrm{grid}}(t)$ is the grid-connected wind power, $P_{\mathrm{wind,q}}(t)$ is the curtailed wind power.

$$\begin{cases} P_{\mathrm{th},m}^{\min}(t) \le P_{\mathrm{th},m}(t) \le P_{\mathrm{th},m}^{\max}(t) \\ -\Delta P_{\mathrm{th},m,\mathrm{dn}}(t) \le P_{\mathrm{th},m}(t) - P_{\mathrm{th},m}(t-1) \le \Delta P_{\mathrm{th},m,\mathrm{up}}(t) \end{cases} \tag{26}$$

ISSN: 2710-0588

where $P_{\mathrm{th},m}^{\min}(t)$ and $P_{\mathrm{th},m}^{\max}(t)$ are the minimum and maximum outputs of thermal unit m, respectively. $\Delta P_{\mathrm{th},m,\mathrm{up}}(t)$ and $\Delta P_{\mathrm{th},m,\mathrm{dn}}(t)$ are the upward and downward ramping rates of thermal unit m.

(3) EV cluster and BCSS operation power constraint

$$0 \le P_{\mathrm{BCSS}}(t) \le P_{\mathrm{CS}}^{\max}(t) + P_{\mathrm{EV},t}^{\mathrm{cha},\max} \tag{27}$$

where $P_{\mathrm{CS}}^{\max}(t)$ is the upper limit of the replacement battery capacity in the BCSS.

(4) Spinning reserve capacity constraint

$$\begin{cases} \sum_{m=1}^{M} P_{\mathrm{th},m,\mathrm{dn}}(t) \ge P_{\mathrm{sys,dn}}(t) \\ \sum_{m=1}^{M} P_{\mathrm{th},m,\mathrm{up}}(t) \ge P_{\mathrm{sys,up}}(t) \end{cases} \tag{28}$$

where $P_{\mathrm{th},m,\mathrm{up}}(t)$ and $P_{\mathrm{th},m,\mathrm{dn}}(t)$ are the upward and downward spinning reserves provided by thermal unit m, $P_{\mathrm{sys,up}}(t)$ and $P_{\mathrm{sys,dn}}(t)$ are the upward and downward spinning reserves required by the system.

6. Case Analysis

6.1. Parameter Settings

The case includes one wind farm with an installed capacity of 300 MW; one EV BCSS, with an average daily number of EVs charging of 1000 and 500 battery swaps in swap mode; four conventional thermal power units [26-28], the operating parameters of the thermal units are shown in Tab. 1; other parameter values are shown in Tab. 2; the day-ahead forecasted grid-connected wind power output for a typical day (1-hour resolution) is shown in Fig. 2.

The NSGA-II algorithm is used for solution, with a population size N of 500 and a maximum number of iterations of 100. The selection strategy adopts tournament selection. The mutation strategy uses Gaussian mutation with a mutation probability of 0.08. The crossover strategy uses two-point crossover with a crossover probability of 0.8 [29-30].

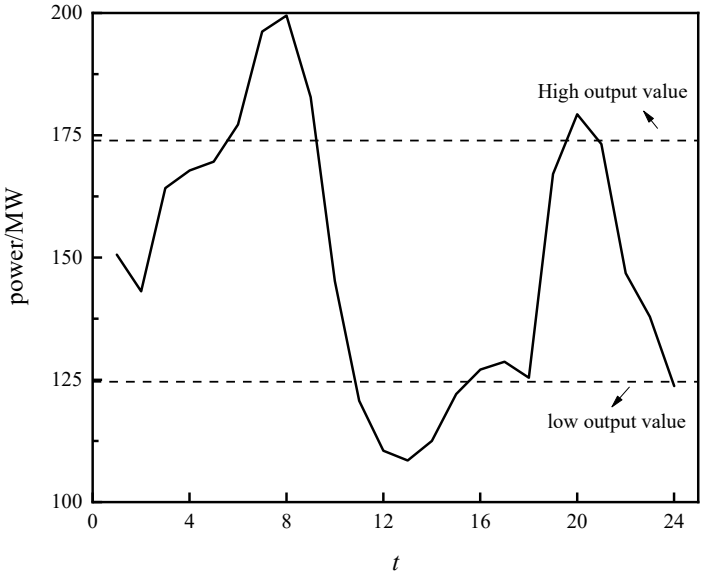

Figure 2. Prediction curve of grid-connected wind power before the day

ISSN: 2710-0588

Table 1. Operating parameters of thermal power units

Unit	Max output /MW	Min output /MW	Ramp rate /MWh^{-1}	Carbon emission intensity /(t·MWh^{-1})	Cost coefficients		
					a_m/yuan·MW^{-2}	b_m/yuan·MW^{-1}	c_m/yuan
G1	200	50	100	0.97	0.00145	200	75
G2	35	10	18	0.96	0.0015	225	167
G3	50	15	25	1.08	0.0023	100	1250
G4	40	10	15	1.15	0.0009	150	500

Table 2. Parameter settings for BCSS and other system components

Item	Value	Item	Value
EV charging efficiency/ (%)	95	Battery depreciation cost/ (yuan·MW^{-1})	80
Charging power/ (kW)	20	Wind curtailment penalty cost coefficient/(yuan·MW^{-1})	100
Battery capacity/ (kWh)	82	Wind power O&M cost coefficient/(yuan·MW^{-1})	30
Electricity consumption per 100 km/ (kWh)	20.5	Carbon emission quota/(t·MWh^{-1})	0.7
BCSS max output power/ (MW)	20	Unit carbon emission trading price/(yuan·t^{-1})	120

Based on the wind power output in Fig. 2, the 24-hour dynamic TOU electricity price considering wind power accommodation can be formulated: periods with high wind power output (06:00–09:00, 19:00–21:00) are set as low-price periods with an electricity price of 0.6 yuan; periods with low wind power output (11:00–15:00) are set as high-price periods with an electricity price of 1.2 yuan; the remaining periods are flat-price periods with an electricity price of 0.8 yuan. This strategy fully utilizes charging cost differences to guide users to reduce charging costs, thereby encouraging EV clusters and BCSS to shift their charging load to high wind power output (low-price) periods and improve wind power accommodation.

6.2. Analysis of Uncoordinated EV Charging

Monte Carlo simulation is used to calculate the uncoordinated charging load demand of X EVs. The charging load of different scales of EV clusters under uncoordinated charging is obtained. To quantitatively analyze the adverse impact of uncoordinated charging of different numbers of EVs on the grid load, it is superimposed on the regional grid base load to obtain the equivalent total load power curve, as shown in Fig. 3. Quantitative analysis of the equivalent total grid load in terms of load peak, load variance, and peak-valley difference rate is presented in Tab. 3.

Table 3. Quantitative analysis of equivalent total grid load

EVs	P_{peak} /MW	σ^2 /(MW)^2	φ /%
X=0	325.81	776.68	32.98
X=200	326.97	790.23	33.21
X=400	328.36	798.35	33.30
X=600	329.48	809.17	33.50
X=800	330.69	812.54	33.53
X=1000	332.84	836.83	33.96

ISSN: 2710-0588

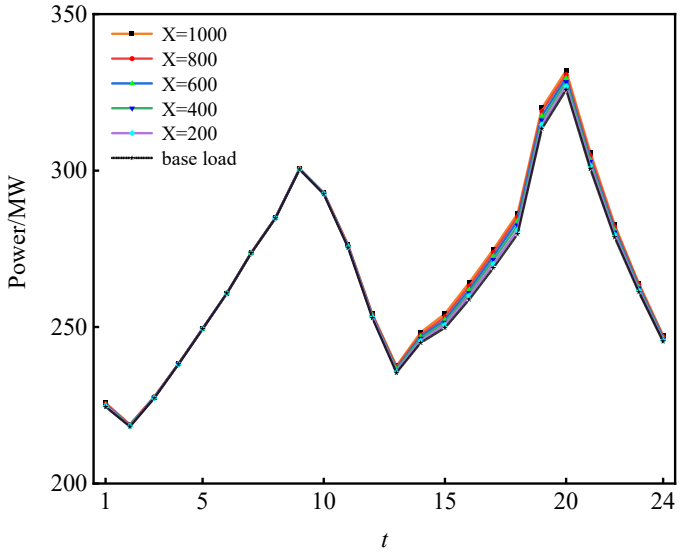

Figure 3. Equivalent load of disorderly charging grid of different Evs

As shown in Fig. 3, the uncoordinated charging load peak period of EV clusters (15:00–22:00) highly coincides with the peak period of the grid base load. In this case, if the cluster charging load is not regulated and is directly connected to the grid, it will result in a severe "peak upon peak" phenomenon. From the quantitative analysis in Tab. 3, it can be seen that as the scale of EV clusters increases, the grid's load peak, load variance, and peak-valley difference rate also increase, leading to increased grid peak-shaving pressure and security operation risks, further complicating grid dispatch.

Table 4. Comparison of simulation results for different scenarios

Scenario	Comprehensive cost /10^4 yuan	Wind power		Thermal power		Load peak-valley characteristics		
		Grid-connected energy /MWh	Curtailment rate /%	Grid-connected energy /MWh	Carbon emissions /t	P_{peak} /MW	P_{vall} /MW	Peak-valley difference /MW
1	68.60	3579.68	0.21	2894.80	1966.57	327.07	234.82	92.25
2	73.84	3175.23	11.45	3194.65	2587.86	325.78	218.20	107.58

6.3. Simulation Results and Analysis

To demonstrate the effectiveness of the proposed low-carbon economic dispatch model and strategy, a comparative analysis is conducted. Scenario 1 includes carbon trading cost constraints and considers ordered charging scheduling of EVs and BCSS. Scenario 2 has no carbon trading cost constraints and does not consider ordered charging scheduling of EVs and BCSS. Tab. 4 presents the simulation results for the two scenarios.

According to Tab. 4, compared to Scenario 2, after introducing carbon trading cost constraints in Scenario 1, the grid load peak-valley difference decreases by 15.33 MW; grid-connected wind power (i.e., wind power accommodation) increases by 404.45 MWh, and the curtailment rate decreases by 11.24%; carbon emissions decrease by 621.29 t; the comprehensive operating cost decreases by 52,400 yuan. The above results indicate that the proposed strategy effectively reduces the grid peak-valley difference, promotes wind power accommodation, reduces carbon emissions from thermal power units, and achieves low-carbon economic operation of the regional grid.

To explore the operational mechanism by which carbon trading cost constraints promote emission reduction of thermal power units, Fig. 4 shows the output of thermal units G1 and G3 under carbon trading cost constraints. It can be seen from Fig. 4 that without carbon trading

ISSN: 2710-0588

costs, G1 and G3, which have relatively low and similar operating costs, are given priority for output, with carbon emission intensities of 0.97 t/(MWh) and 1.08 t/(MWh), respectively, while G2 and G4, with higher operating costs, remain offline. After introducing carbon trading costs, G2 and G4 remain offline due to their high operating costs; G3 reduces output due to rising total costs and eventually shuts down. In contrast, G1 increases output due to its better economic performance. From Tab. 4, thermal power output decreases by 299.85 MWh. The analysis shows that carbon trading cost constraints can optimize the output structure of generating units and indirectly enhance the accommodation capacity of regional grid wind power.

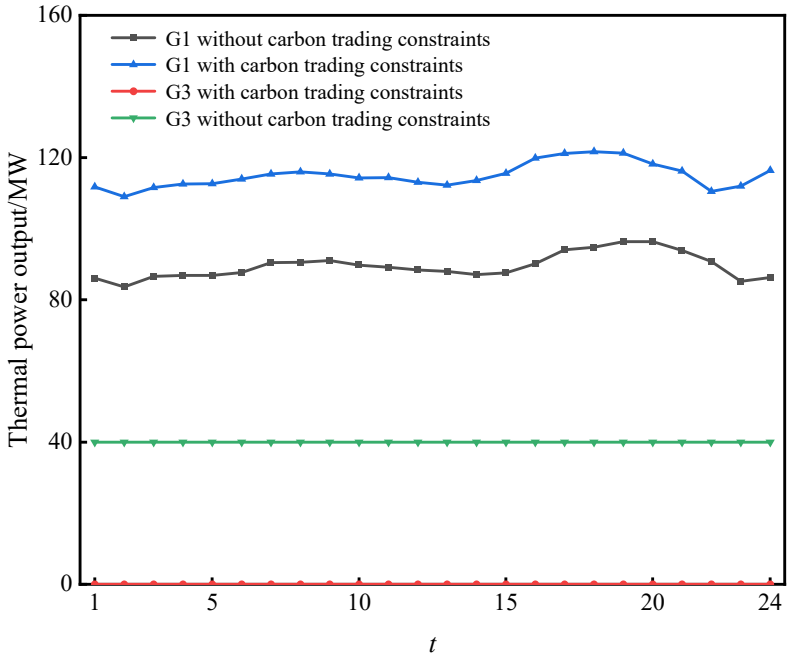

Figure 4. Output of units with and without carbon trading constraints

Fig. 5 and Fig. 6 present the operating results of wind power output, thermal power output, and grid equivalent load for Scenario 1 and Scenario 2, respectively. Analysis of Fig. 5 and Fig. 6 shows that the coordinated output of wind and thermal power enables stable and adjustable operation of generating units, meeting grid load demand and achieving system power balance. In the absence of carbon trading costs, although thermal power as an auxiliary source can provide sufficient spinning reserve for the system to cope with wind power and load uncertainties, during nighttime load valleys or periods of large wind speed fluctuations, the system tends to prioritize thermal units with stable output and low costs to ensure power supply economy and stability, resulting in reduced grid-connected space for wind power. Curtailment is most severe during periods 01:00–07:00 and 19:00–24:00. In contrast, after introducing carbon trading costs, thermal units actively reduce output during periods of high curtailment or low grid load, freeing up more grid space for wind power and increasing wind power accommodation. During periods of low wind power output or high grid load, thermal units increase output to meet grid load demand.

ISSN: 2710-0588

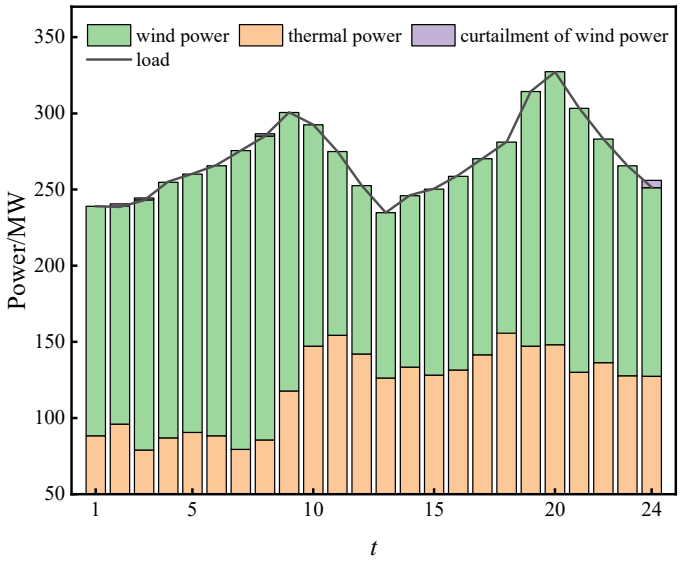

Figure 5. Simulation results of scenario 1

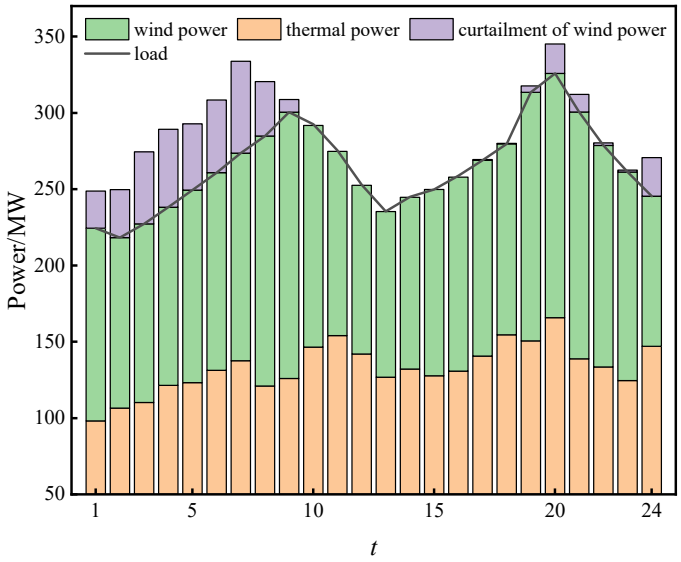

Figure 6. Simulation results of scenario 2

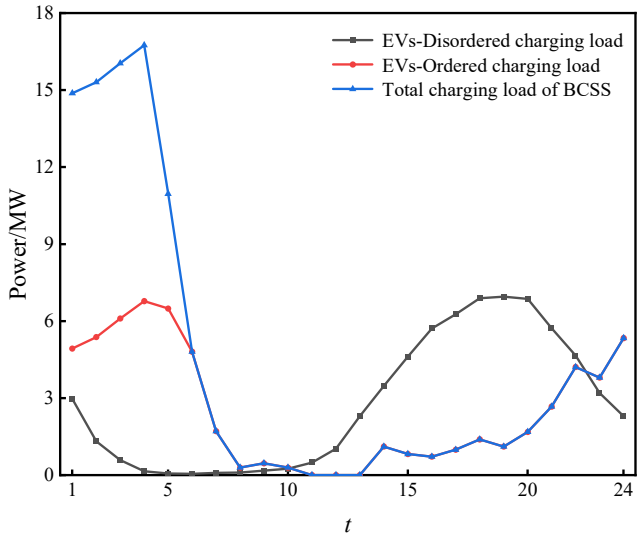

Figure 7. Load power curve of EVs and BCSS

ISSN: 2710-0588

Fig. 7 shows the load power curves of the EV cluster and BCSS. Analysis of Fig. 7 reveals that the energy storage preparation of replacement batteries in the BCSS is centrally regulated in the period 01:00–06:00. Through the ordered charging control model for EVs, the concentrated uncoordinated charging period (11:00–22:00) is effectively shifted to periods 22:00–24:00 and 1:00–8:00, effectively transferring the EV charging load. Furthermore, analysis shows that these periods coincide with high wind curtailment periods. By utilizing the ordered charging load of EVs and BCSS, the originally wasted wind power resources are locally absorbed, achieving efficient utilization of curtailed wind power. This also validates the effectiveness of the proposed ordered charging control model for EVs and the TOU pricing strategy considering wind power accommodation.

7. Conclusion

Based on the paper, the main conclusions are summarized as follows:

A dynamic time-of-use electricity pricing strategy based on wind power output is proposed, effectively shifting EV charging load to high-wind periods and increasing wind power accommodation by 404.45 MWh while reducing the curtailment rate by 11.24%.

Introducing carbon trading costs reduces thermal power output by 299.85 MWh and carbon emissions by 621.29 t, while also optimizing the unit output structure and indirectly enhancing wind power integration.

References

[1] Wang X J, Liu P, Li R C, et al. Research progress and prospect of advanced power generation technology under the goal of carbon peak and carbon neutrality. Thermal Power Generation, 2022, 51(01): 52-59.

[2] Cui Y, Guo F Y, Fu X B, et al. Source-load coordinated optimal dispatch of integrated energy system promoting wind power accommodation by supply-use conversion. Power System Technology, 2022, 46(04): 1437-1447.

[3] Malika K B, Pattanaik V, Panda S, et al. A critical review of distribution system planning: Optimal placement and sizing of distributed generation and energy storage devices in microgrids. Energy Strategy Reviews, 2025, 62: 101947.

[4] Ma Y P. Optimal capacity configuration of hybrid energy storage in microgrid considering electric vehicle dispatch. Power System Protection and Control, 2017, 45(23): 98-107.

[5] Niu M, Ji R, Pang H, et al. A two-stage optimization framework for microgrid operation with EV ordered charging and hydrogen-battery co-storage. Journal of Energy Storage, 2025, 129: 117165.

[6] Wang H, Li X Y, Wang B Q, et al. Reliability evaluation of distribution network with distributed generation and electric vehicles. Journal of Chongqing University, 2024, 47(01): 115-126.

[7] Bahmani H M, Shayan E M, Mishra K D. Quantifying the impact of electricity pricing on electric vehicle user behavior: a V2G perspective for smart grid development. Energy Sources, Part A: Recovery, Utilization, and Environmental Effects, 2024, 46(1): 4524-4542.

[8] Wang S, Liu B, Hua Y, et al. Dispatchable capability of aggregated electric vehicle charging in distribution systems. Energy Engineering, 2024, 122(1): 129-152.

[9] Guo Y N, Liao K, Yang J W, et al. Capacity optimization method for electric vehicle battery swapping station considering distribution network resilience enhancement. Power System Technology, 2025, 49(02): 470-480.

[10] Kong S F, Hu Z J, Xie S Y, et al. Two-stage robust planning model and its solution method for active distribution network with electric vehicle charging stations. Transactions of China Electrotechnical Society, 2020, 35(5): 1093-1105.

[11] Ma M, Ren Z W, Liu L C, et al. Ordered charging control strategy for electric vehicles considering renewable energy accommodation. Acta Energiae Solaris Sinica, 2024, 45(08): 94-103.

ISSN: 2710-0588

[12] Ji X, Li M, Yue Z, et al. Renewable energy consumption strategies for electric vehicle aggregators based on a two-layer game. Energies, 2024, 18(1): 80-80.

[13] Cui Y, Jiang T, Zhong W Z, et al. Economic dispatch method of regional integrated energy system considering electric vehicle and heat pump for promoting wind power consumption. Electric Power Automation Equipment, 2021, 41(02): 1-7.

[14] Shu Z Y, Liu W C, Li H Q, et al. Ordered charging and discharging strategy for electric vehicles based on cooperative game and dynamic time-of-use electricity price. Electric Power Engineering Technology, 2025, 44(03): 179-187.

[15] Yang J X, Zhou L, Zhang Y J, et al. Ordered EV charging considering time-varying price and transition probability under dedicated transformer sharing mode. Electric Power Automation Equipment, 2020, 40(10): 173-180, 193.

[16] Zeng X K, Yang P, Liu L Y, et al. Optimal regulation strategy of EV charging and swapping station in electricity spot market environment. Electric Power Automation Equipment, 2022, 42(10): 38-45.

[17] Wang Y F, Wang X H, Lei X S. Optimal operation strategy under integrated service mode of prefabricated substation and EV charging/swapping station. Southern Power System Technology, 2022, 16(05): 61-70.

[18] Yue X, Fang M Q, Liu J Y, et al. Distributed dispatch of multiple energy systems considering carbon trading. CSEE Journal of Power and Energy Systems, 2023, 9(02): 459-469.

[19] Jin J, Zhou P, Li C, et al. Low-carbon power dispatch with wind power based on carbon trading mechanism. Energy, 2019, 170: 250-260.

[20] Wang J, Huang K R, Xu X, et al. Orderly charging of electric vehicles based on stepped carbon price and adaptive time-of-use electricity price. Electric Power Automation Equipment, 2024, 44(02): 64-71.

[21] Cui Y, Zeng P, Zhong W Z, et al. Low-carbon economic dispatch of electricity-gas-heat integrated energy system based on stepped carbon trading. Electric Power Automation Equipment, 2021, 41(03): 10-17.

[22] Xiao Q Y, Yang K, Song Z X. Dispatch strategy of integrated energy system in industrial park considering carbon trading and EV charging load. High Voltage Engineering, 2023, 49(04): 1392-1401.

[23] Huang Z, Wang Y, Liu C, et al. Low-carbon and optimized dispatching of regional integrated energy systems, taking into account the uncertainties of wind–solar power and dynamic hydrogen prices. Energies, 2025, 18(23): 6265-6265.

[24] Wu X, Liang K X, Jiao D, et al. Group coordination method of air conditioners for clean energy tracking. Automation of Electric Power Systems, 2020, 44(11): 68-77.

[25] Zhang C, Kuang Y, Zou F M, et al. Low-carbon economic dispatch of integrated energy system considering wind and solar uncertainty and electric vehicles. Electric Power Automation Equipment, 2022, 42(10): 236-244.

[26] Liu R L, Yu Y, Liu J, et al. Electric vehicle charging load prediction based on improved Monte Carlo algorithm. Zhejiang Electric Power, 2025, 44(08): 15-23.

[27] Wang S Q, Duan J D, Duan Z Y. Collaborative optimization strategy of "wind power-grid-EV charging and swapping station" considering wind power accommodation. Thermal Power Generation, 2023, 52(03): 112-120.

[28] Zhu Y S, Chang W, Wu D Y, et al. Master-slave game optimization dispatch strategy considering interaction between integrated charging-swapping-storage station and electric vehicles. Power System Protection and Control, 2024, 52(07): 157-167.

[29] Chen J, Zhang X D, Li L Y, et al. Two-stage game collaborative dispatch strategy for shared EV charging based on electricity-carbon joint mechanism. Power System Technology, 2024, 48(09): 3584-3594.

[30] Yu Y F, Liu B L. Environmental economic dispatch optimization of power load based on improved NSGA-II algorithm. Jiangxi Electric Power, 2024, 48(03): 8-11.